

## Synthesis and characterization of cyano-substituted pyridine derivatives for applications as exciton blockers in photovoltaic devices†

Juanjuan You,<sup>abc</sup> Ming-Fai Lo,<sup>b</sup> Weimin Liu,<sup>a</sup> Tsz-Wai Ng,<sup>b</sup> Shiu-Lun Lai,<sup>b</sup> Pengfei Wang<sup>\*a</sup> and Chun-Sing Lee<sup>\*b</sup>

Received 18th October 2011, Accepted 5th January 2012

DOI: 10.1039/c2jm15287h

A new class of cyano-substituted pyridine derivatives have been synthesized and characterized. The relationship between their chemical structures, energy gap, energy levels, electron mobility and device performance was studied systematically by applying the new materials as EBL in standard CuPc/C<sub>60</sub>/EBL organic photovoltaic (OPV) devices. Their properties fulfill all the requirements for a good EBL material, such as a wide energy gap ( $E_g$ , 3.12–3.50 eV), a deep highest occupied molecular orbital (HOMO, 6.71–7.80 eV) energy level, a high electron mobility (in the order of  $10^{-5}$  cm<sup>2</sup> V<sup>-1</sup> s<sup>-1</sup>) and a high glass transition temperature ( $T_g$ , 139–189 °C), thus most of them show performances surpassing that of BCP. In particular, one device shows an efficiency of 2.12% and a half-efficiency lifetime of 340 h, which are, respectively, 44% and more than 5 times better than those (1.47%, 60 h) of the BCP-based device. Furthermore, we found that the lowest unoccupied molecular orbital (LUMO) energy level of the EBL can also influence the leakage current and thus the efficiency of the OPV devices. It is expected that these studies would provide useful guidance for designing high-performance EBL materials.

## 1. Introduction

Organic photovoltaic (OPV) devices have attracted much attention recently for their various merits including low manufacturing cost, slight weight, large area and potential flexibility.<sup>1,2</sup> In the past decade, most research efforts have been focussed on enhancing power conversion efficiency. One of the most important progresses is the introduction of an exciton-blocking layer (EBL), which can prevent the active layer from being damaged in the vacuum thermal-deposition process of the metal electrode and reduce the loss of excitons *via* quenching by keeping the excitons away from the metal cathode.<sup>3,4</sup> In addition, other approaches including the introduction of various anode buffer layers,<sup>5–7</sup> bulk heterojunction,<sup>3,8</sup> and high performance materials *etc.*<sup>9–12</sup> have increased the power conversion efficiency to a level where commercial applications become viable.<sup>13</sup>

However, the operational stabilities of such devices are still far below requirements of most applications. While the stability problem is clearly a pressing issue, so far not many systematic studies have been carried out. Actually, the authors have shown that oxygen species from the ITO is one factor that causes degradation of devices using C<sub>60</sub>.<sup>7,14</sup> Substantially improved device stability has been achieved by inserting a fluorocarbon layer between the ITO anode and the photoactive organic layers.<sup>7</sup> On the other hand, crystallization of the bathocuproine (BCP) – the most commonly used EBL under the cathode – has been identified as another important cause of degradation.<sup>15</sup> To address this problem, several other organic materials, such as Alq<sub>3</sub> and its derivatives, have been used instead of BCP.<sup>15–21</sup> While these materials do offer considerable stability enhancement, their electrical performances are similar or only slightly better than BCP. Up til now, there has been no report on a BCP replacement which can simultaneously enhance both the stability and efficiency considerably. It is thus highly desirable to develop a high performance EBL for replacing BCP.

In general a good EBL material should have 1) a wide energy gap ( $E_g$ ) to block excitons diffusion to the cathode; 2) a deep highest occupied molecular orbital (HOMO) energy level to block hole leakage to the cathode; 3) a high electron mobility for low electrical resistance; 4) a low optical absorption to minimize photon loss and 5) a high glass transition temperature ( $T_g$ ) for thermal stability.<sup>22–26</sup> We have previously used a pyridine derivative *p*-PPTNT as an electron-transporting and hole-blocking layer in high-performance deep blue OLEDs.<sup>27,28</sup> It appears that the properties of *p*-PPTNT do fulfill all the requirements for

<sup>a</sup>Key Laboratory of Photochemical Conversion and Optoelectronic Materials Technical Institute of Physics and Chemistry, Chinese Academy of Sciences, No. 29, Zhongguancun East Road, Haidian District, Beijing, 100190, P. R. China. E-mail: wangpf@mail.ipc.ac.cn; Fax: (+86) 10-8254-3512

<sup>b</sup>Center of Super-Diamond and Advanced Films (COSDAF), Department of Physics and Materials Science, City University of Hong Kong, Tat Chee Avenue, Kowloon, Hong Kong SAR, P. R. China. E-mail: apcslee@cityu.edu.hk

<sup>c</sup>Graduate University of Chinese Academy of Sciences, Beijing, 100190, P. R. China

† Electronic supplementary information (ESI) available: thermal properties measurements; electron mobility measurements; molecular structure of *p*-MPyCN's intermediate product. See DOI: 10.1039/c2jm15287h

a good EBL material and similar pyridine derivatives might have good potential for this application.

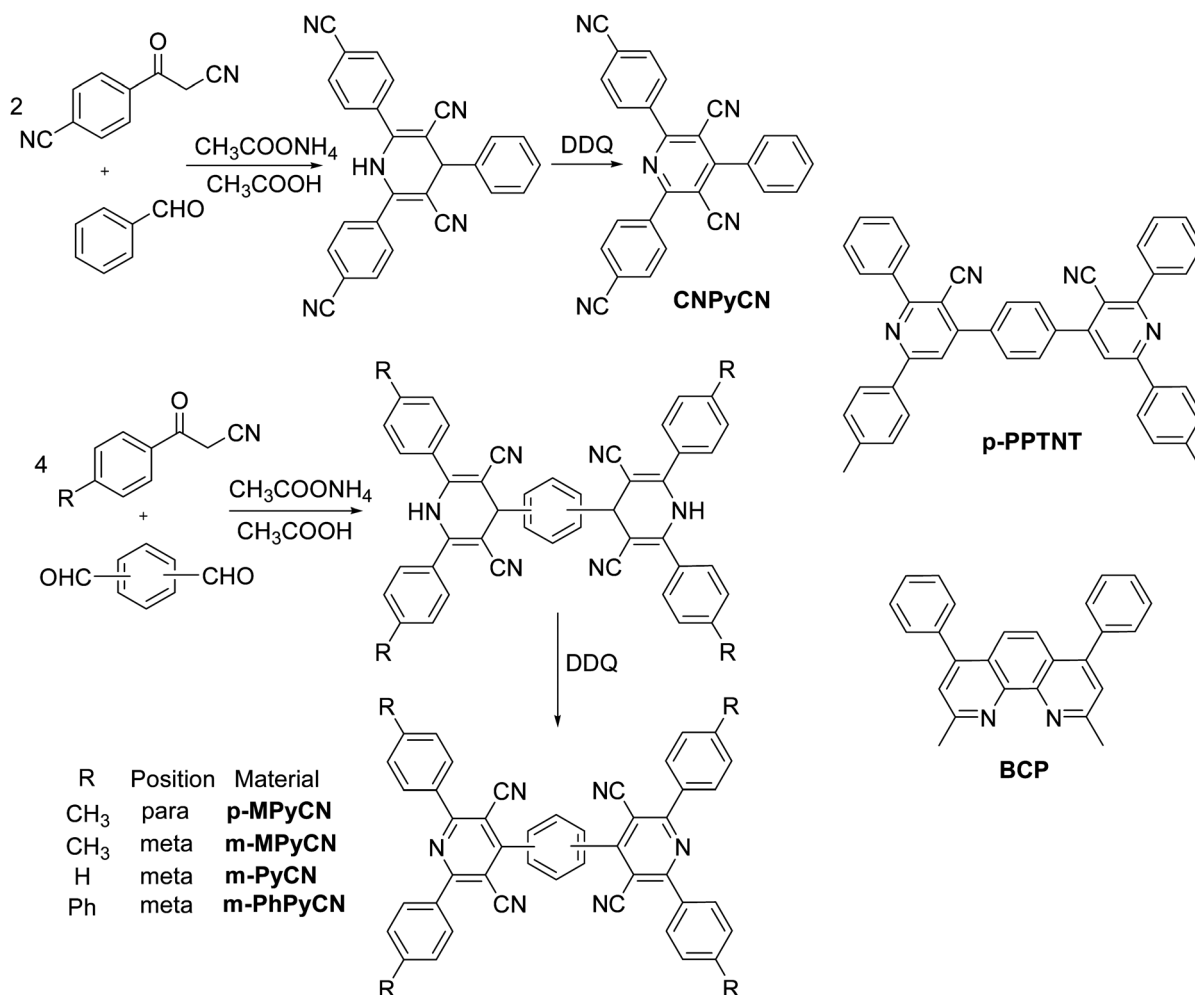
In this work, we designed and synthesized a series of cyano-substituted pyridine derivatives with structures as shown in Scheme 1. The design concept is based on the fact that by introducing more cyano groups on the pyridine moiety, the HOMO energy level can be drawn further downwards. The added cyano groups would also increase the steric hindrance and perturb the molecular planarity,<sup>29–32</sup> leading to wider energy gaps. Performances of the new compounds were studied by applying them as EBL in standard CuPc/C<sub>60</sub>/EBL devices. Most of the new compounds show performances surpassing that of BCP. In particular, the device using *m*-MPyCN as EBL shows an efficiency of 2.12% and a half-efficiency lifetime of 340 h, which are, respectively, 44% and more than 5 times better than those (1.47%, 60 h) of the BCP-based reference device. Furthermore, in addition to the EBL requirements mentioned above, we also found that the energy of the lowest unoccupied molecular orbital (LUMO) of the EBL can influence the leakage current and thus the efficiency of the OPV devices. Based on these results, we analyzed the relationship between chemical structures, energy gap, energy levels, electron mobility and performance of these cyano-substituted pyridine derivatives. It is expected that these

results would provide useful guidance for designing high-performance EBL materials.

## 2. Experimental section

### 2.1 Synthesis

The synthetic routes of the cyano-substituted pyridine derivatives are shown in Scheme 1. A representative synthetic procedure for *m*-MPyCN is as follows: 4-methylbenzoylacetone nitrile (0.95 g, 6 mmol) and isophthalaldehyde (0.20 g, 1.5 mmol) were dissolved in 30 mL of glacial acetic acid containing ammonium acetate (1.15 g, 15 mmol). The mixture was refluxed under an air atmosphere at 120 °C. After three hours, a yellow precipitate was collected and washed with glacial acetic acid. The crude precipitate was then added to 30 mL of glacial acetic acid. Under rapid stirring, 2,3-dichloro-5,6-dicyano-*p*-benzoquinone (DDQ, 0.80 g, 3.5 mmol) was added to the glacial acetic acid solution. The mixture was refluxed for one hour at 120 °C. After cooling to room temperature, the reaction mixture was filtered and washed with methanol to obtain a white powder. The white powder was further purified by column chromatography with dichloromethane as an eluting agent. Finally, 0.78 g white powder of *m*-MPyCN was obtained (yield 75%).



**Scheme 1** Molecular structures (*p*-PPTNT and BCP are included for reference) and synthetic routes of the new cyano-substituted pyridine derivatives.

**4,4'-(1,3-phenylene) bis(2,6-dip-tolylpyridine-3,5-dicarbonitrile) (*m*-MPyCN).**  $^1\text{H}$  NMR (400 MHz,  $\text{CDCl}_3$ ,  $\delta$ ): 8.00 (d, 8H,  $J = 8.2$ ), 7.90 (s, 4H), 7.35(d, 8H,  $J = 8.1$ ), 2.45 (s, 12H).  $^{13}\text{C}$  NMR (400 MHz,  $\text{CDCl}_3$ ,  $\delta$ ): 163.4, 158.8, 142.2, 134.8, 133.7, 131.5, 130.3, 129.7, 129.6, 115.9, 105.3, 21.7. HRMS (EI,  $m/z$ ): [ $\text{M}^+$ ] calcd for  $\text{C}_{48}\text{H}_{32}\text{N}_6$ : 692.2688; found: 692.2700. Anal. calcd. for  $\text{C}_{48}\text{H}_{32}\text{N}_6$ : C 83.21, H 4.66, N 12.13; Found: C 83.22, H 4.71, N 12.13.

**4,4'-(1,3-phenylene) bis(2,6-diphenylpyridine-3,5-dicarbonitrile) (*m*-PyCN).**  $^1\text{H}$  NMR (400 MHz,  $\text{CDCl}_3$ ,  $\delta$ ): 8.09 (m, 8H), 7.94 (s, 4H), 7.58(m, 12H).  $^{13}\text{C}$  NMR (400 MHz,  $\text{CDCl}_3$ ,  $\delta$ ): 163.6, 158.7, 136.4, 134.8, 131.7, 130.5, 129.8, 129.6, 129.0, 115.6, 106.1. HRMS (EI,  $m/z$ ): [ $\text{M}^+$ ] calcd for  $\text{C}_{44}\text{H}_{24}\text{N}_6$ : 636.2062; found: 636.2069. Anal. calcd. for  $\text{C}_{44}\text{H}_{24}\text{N}_6$ : C 83.00, H 3.80, N 13.20; Found: C 82.91, H 3.80, N 13.22.

**4,4'-(1,3-phenylene) bis(2,6-di(biphenyl-4-yl)pyridine-3,5-dicarbonitrile) (*m*-PhPyCN).**  $^1\text{H}$  NMR (400 MHz,  $\text{CDCl}_3$ ,  $\delta$ ): 8.24 (d, 8H,  $J = 8.4$ ), 7.98 (s, 4H), 7.80 (d, 8H,  $J = 8.4$ ), 7.69 (m, 8H), 7.49 (m, 8H), 7.42 (d, 4H,  $J = 7.2$ ).  $^{13}\text{C}$  NMR (400 MHz,  $\text{CDCl}_3$ ,  $\delta$ ): 163.0, 159.0, 144.6, 140.0, 135.2, 134.8, 131.7, 130.5, 130.3, 129.6, 129.1, 128.3, 127.7, 127.4, 115.8, 105.7. MS (MALDI-TOF,  $m/z$ ): [ $\text{M} + \text{Na}$ ] $^+$  calcd for  $\text{C}_{68}\text{H}_{40}\text{N}_6$ : 940.3314; found: 963.4. Anal. calcd. for  $\text{C}_{68}\text{H}_{40}\text{N}_6$ : C 86.79, H 4.28, N 8.93; Found: C 86.47, H 4.49, N 8.69.

**2,6-bis (4-cyanophenyl)-4-phenylpyridine-3,5-dicarbonitrile (CNPyCN).**  $^1\text{H}$  NMR (400 MHz,  $\text{CDCl}_3$ ,  $\delta$ ): 8.16 (d, 4H,  $J = 8.4$ ), 7.88 (d, 4H,  $J = 8.4$ ), 7.66 (m, 5H).  $^{13}\text{C}$  NMR (400 MHz,  $\text{CDCl}_3$ ,  $\delta$ ): 161.7, 161.1, 140.0, 132.8, 131.8, 130.3, 129.6, 128.9, 118.0, 115.5, 115.0, 107.7. HRMS (EI,  $m/z$ ): [ $\text{M}^+$ ] calcd for  $\text{C}_{27}\text{H}_{13}\text{N}_5$ : 407.1171; found: 407.1167. Anal. calcd. for  $\text{C}_{27}\text{H}_{13}\text{N}_5$ : C 79.59, H 3.22, N 17.19; Found: C 79.35, H 3.37, N 16.94.

**4,4'-(1,4-phenylene) bis(2,6-dip-tolylpyridine-3,5-dicarbonitrile) (*p*-MPyCN).** HRMS (EI,  $m/z$ ): [ $\text{M}^+$ ] calcd for  $\text{C}_{48}\text{H}_{32}\text{N}_6$ : 692.2688; found: 692.2698. Anal. calcd. for  $\text{C}_{48}\text{H}_{32}\text{N}_6$ : C 83.21, H 4.66, N 12.13; Found: C 82.21, H 4.70, N 11.86. Data for  $^1\text{H}$  NMR and  $^{13}\text{C}$  NMR were not observed because of its insolubility in commonly used reagents. Therefore, the molecular structure and identification for its intermediate product are shown in the ESI (see Scheme S1†).

## 2.2 Device fabrication

OPV devices were fabricated on patterned ITO-coated glass substrates with a sheet resistance of  $30 \Omega/\square$ . The substrates were cleaned with Decon 90, rinsed in de-ionized water, dried in an oven, and finally exposed to UV-ozone for about 30 min. The ITO substrates were then immediately transferred into a deposition chamber with a base pressure of  $1 \times 10^{-4}$  Pa. Organic layers were sequentially deposited by conventional thermal evaporation. The deposition rates were monitored using a quartz oscillating crystal and controlled to be  $0.1\text{--}0.2 \text{ nm s}^{-1}$ . Then 150 nm of Al cathode was deposited at a rate of  $0.8\text{--}1.0 \text{ nm s}^{-1}$  through a shadow mask to define an active device area of  $0.12 \text{ cm}^2$ . The devices were immediately transferred to the glove box with

a nitrogen atmosphere and encapsulated by ultraviolet light curing resins.

## 2.3 Device and film characterization

Density–voltage ( $J$ – $V$ ) characteristics of the OPV devices were measured with a programmable Keithley model 237 power source. The current was measured in the dark and under illumination with an intensity of  $100 \text{ mW cm}^{-2}$  from an Oriel 150 W solar simulator with AM1.5G filters. The light intensity was calibrated with a reference Si diode with a KG-5 filter. Absorption spectra of solid-state films deposited on quartz substrates were measured with a Perkin-Elmer Lambda 2S UV–visible spectrophotometer. HOMO energy levels were measured with thin films deposited on ITO glass substrates by ultra-violet photoelectron spectroscopy (UPS) in a VG ESCA-LAB 220i-XL surface analysis system. LUMO energy levels were estimated by subtracting from HOMO with the optical band gap determined from the absorption spectra of the solid-state films.

## 3. Results and discussion

### 3.1 Thermal stability

The thermal properties of the new compounds measured with thermogravimetric analyses (TGA) and differential scanning calorimetry (DSC) are summarized in Table 1 and shown in Fig. S1.† It can be seen that all the bilateral compounds possess higher decomposition temperatures ( $T_{\text{ds}}$ ) than the unilateral compound CNPyCN. Compounds with more cyano groups (*m*-PyCN, *p*-MPyCN, *m*-MPyCN and *m*-PhPyCN) also have higher  $T_{\text{ds}}$  than that of *p*-PPTNT. The  $T_{\text{gs}}$  of these compounds have a consistent trend with that of  $T_{\text{ds}}$ . The  $T_{\text{gs}}$  of CNPyCN and *p*-MPyCN were not observed. The former may have too low a  $T_{\text{g}}$  to be detected, while the latter case is probably due to the more bulky and rigid structure than that of the *meta*-substituted *m*-MPyCN. A similar behavior has also been observed for similar bulky structures such as *para*-substituting fluorene derivatives.<sup>33</sup> The absence of  $T_{\text{g}}$  might be caused by hindering of molecular segmental motion by the bulky and rigid structures. Compared with the widely used BCP (with a  $T_{\text{g}} < 80 \text{ }^\circ\text{C}$ )<sup>15</sup> for EBL, most of our cyano-substituted pyridine derivatives possess considerably better thermal stability.

### 3.2 Absorption properties

Optical absorption properties are important parameters controlling the performance of EBLs in OPV devices. Absorption spectra of solid films of the pyridine derivatives on quartz substrates are shown in Fig. 1a. It can be seen that *p*-PPTNT has a strong absorption band peaking at 290 nm and a shoulder at about 340 nm. The two absorption bands can be assigned to the  $\pi$ – $\pi^*$  transition of the pyridine moiety and intramolecular charge transfer (ICT) state respectively. Comparing to *p*-PPTNT, *p*-MPyCN and *m*-MPyCN have similar structures except for more cyano groups on the pyridine moiety, shoulders peaking at less than 250 nm and strong absorption bands peaking around 313 nm are observed, indicating enhanced intramolecular charge transfer. Moreover, steric hindrance of the cyano groups in *p*-MPyCN and *m*-MPyCN can disturb

**Table 1** Properties of the cyano-substituted pyridine derivatives and referenced BCP

Materials	$T_g/T_m/T_d$ [°C]	$\lambda^{\text{ab. max.}}$ <sup>a</sup> [nm]	HOMO [eV]	LUMO [eV]	$E_g$ [eV]	$\mu_e@6$ V <sup>b</sup> [cm <sup>2</sup> V <sup>-1</sup> s <sup>-1</sup> ]	Reference
BCP	<80/n.a./n.a.	n.a.	-6.50	-3.00	3.50	$6 \times 10^{-7}$	Refs 15, 36
<i>m</i> -PhPyCN	189/342/520	342	-6.71	-3.59	3.12	$4.8 \times 10^{-5}$	This work
<i>p</i> -PPTNT	139/363/388	330	-6.81	-3.57	3.24	$4.5 \times 10^{-5}$	Refs 27, 28
<i>m</i> -MPyCN	149/341/402	312	-6.91	-3.55	3.36	$5.6 \times 10^{-5}$	This work
<i>p</i> -MPyCN	n.a./338/426	313	-6.93	-3.61	3.32	$3.4 \times 10^{-5}$	This work
<i>m</i> -PyCN	141/339/408	295	-7.16	-3.70	3.46	$2.9 \times 10^{-5}$	This work
CNPyCN	n.a./n.a./325	289	-7.80	-4.30	3.50	n.a. <sup>c</sup>	This work

<sup>a</sup>  $\lambda^{\text{ab. max.}}$ : maximum wavelength of absorption (deposited on the quartz substrates). <sup>b</sup>  $\mu_e$ : electron mobility (measured by transient electroluminescence method). <sup>c</sup> Due to the weak EL of CNPyCN, its transient EL signal cannot be detected.

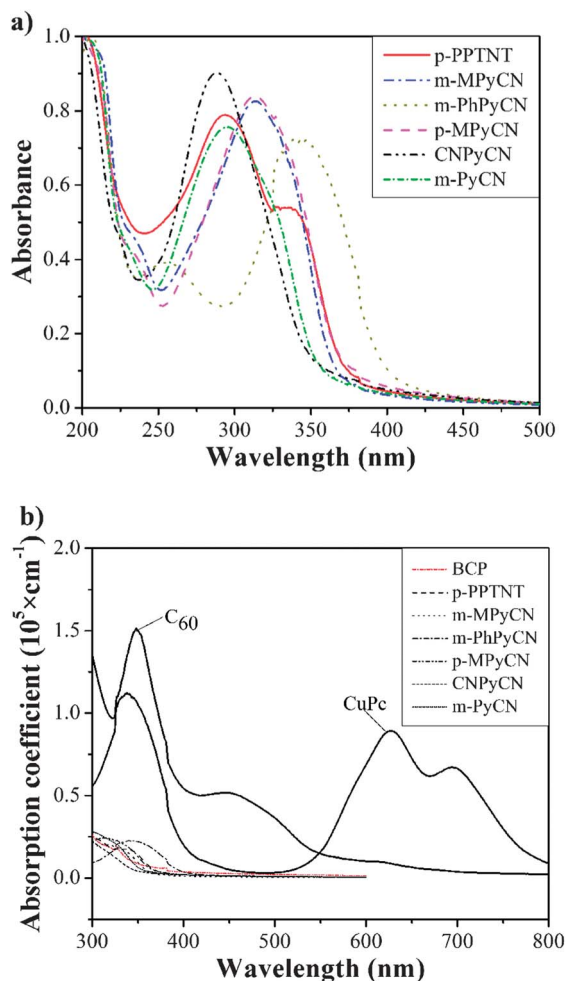


**Fig. 1** a) Normalized absorption spectra of the cyano-substituted pyridine derivatives on quartz substrates. b) Absorption coefficients of the cyano-substituted pyridine derivatives, BCP, CuPc and C<sub>60</sub> on quartz substrates.

molecular planarity leading to a shortened conjugation length and blue-shift of the absorption peaks. On the other hand, replacing the methyl substituent with weaker electron-donating hydrogen or cyano substituents would weaken ICT, resulting in blue-shifted absorption peaks in *m*-PyCN and CNPyCN. On the contrary, by introducing a stronger electron-donating phenyl substituent, two red-shifted absorption peaks centered around

250 nm and 340 nm are found in *m*-PhPyCN, which indicates a higher degree of ICT.

Fig. 1b shows the absorption coefficients of the pyridine derivatives and three other reference materials (BCP, CuPc and C<sub>60</sub>). One key requirement of the EBL is low optical absorption compared to the photo-active components in the OPV device. The pyridine derivatives clearly satisfy this requirement as their absorption coefficients are much lower than those of CuPc and C<sub>60</sub> and are comparable to that of BCP.

### 3.3 Energy level and electron mobility

Energy level as well as electron mobility are also important parameters for EBLs in OPV devices. The HOMO and LUMO energies of the materials as determined by UPS and optical absorption measurements were listed in Table 1. In agreement with our original design concept, by introducing more cyano groups on the pyridine moiety, *p*-MPyCN has a deeper HOMO energy level and a wider  $E_g$  compared to *p*-PPTNT. Meanwhile, the HOMO energy levels of cyano-substituted pyridine derivatives can be tuned, by different substituents, from 6.71 to 7.80 eV with an increased degree of electron-deficiency, indicating better hole-blocking abilities than BCP (with a HOMO energy level of 6.5 eV). In addition, all of them have wide  $E_g$ s larger than 3.0 eV, explaining their abilities for blocking excitons.

The electron mobilities of the cyano-substituted pyridine derivatives were measured using the transient electroluminescence (EL) method.<sup>34,35</sup> As shown in Table 1 and Table S1,<sup>†</sup> the electron mobilities of all the cyano-substituted pyridine derivatives are in the order of  $10^{-5}$  cm<sup>2</sup> V<sup>-1</sup> s<sup>-1</sup>, which are two orders of magnitude higher than that of BCP<sup>36</sup> and facilitate more efficient electron transport through EBLs.

### 3.4 Photovoltaic performances

OPV devices with a structure of ITO/CuPc (35 nm)/C<sub>60</sub> (45 nm)/EBLs (5 nm)/Al (150 nm) were fabricated by using the six pyridine derivatives and BCP as the EBL. For easy reference, the energy levels of the used materials are shown in Fig. 2. Fig. 3 depicts the current density–voltage ( $J$ – $V$ ) characteristics of the OPV devices with different EBLs under 1 Sun AM 1.5G (AM: air mass, G: global) simulated solar illumination. Key device performance parameters including short-circuit current ( $J_{SC}$ ), open-circuit voltage ( $V_{OC}$ ), fill factor (FF), shunt resistance ( $R_{Sh}$ ), series resistance ( $R_S$ ), and power conversion efficiency (PCE) are summarized in Table 2. For the first approximation,

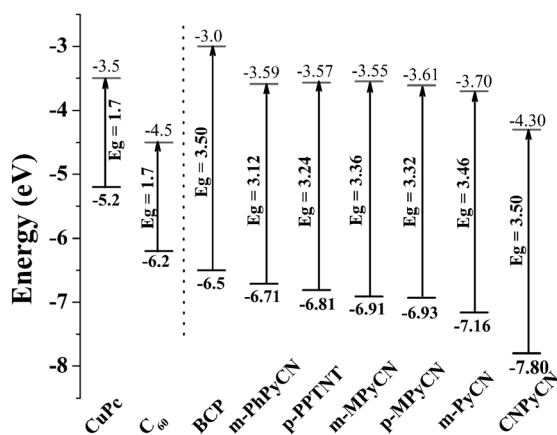


Fig. 2 The energy levels of the materials used.

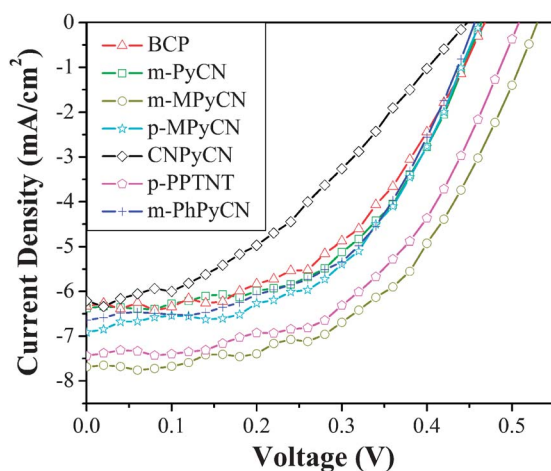


Fig. 3 The current density–voltage ( $J$ – $V$ ) characteristics of the OPVs with different EBLs under 1 Sun AM 1.5G simulated solar illumination.

$R_S$  and  $R_{Sh}$  were estimated from the inverse slope of the  $J$ – $V$  characteristic at zero  $J$  and  $V$ , respectively.<sup>37,38</sup> It can be seen that the devices using  $p$ -PPTNT ( $J_{SC} = 7.44 \text{ mA cm}^{-2}$ ,  $V_{OC} = 0.51 \text{ V}$ ,  $FF = 0.51$ ;  $PCE = 1.93\%$ ) and  $m$ -MPyCN ( $J_{SC} = 7.69 \text{ mA cm}^{-2}$ ,  $V_{OC} = 0.53 \text{ V}$ ,  $FF = 0.52$ ;  $PCE = 2.12\%$ ) have considerably better performance than the reference device using BCP ( $J_{SC} = 6.33 \text{ mA cm}^{-2}$ ,  $V_{OC} = 0.47 \text{ V}$ ,  $FF = 0.50$ ,  $PCE = 1.47\%$ ) as the EBL. In particular, the  $PCE$  of the  $m$ -MPyCN device is about 44% higher than that of the BCP device. Furthermore, devices using  $m$ -PhPyCN,  $p$ -MPyCN and  $m$ -PyCN also show higher  $PCE$  (1.60%, 1.63% and 1.55%, respectively) than that of the

BCP device. Of all the devices using the new compounds, only the CNPyCN device shows a lower  $PCE$  (1.07%) than the reference BCP device. Though CNPyCN has the deepest HOMO and the widest  $E_g$ , the performance of its device is obviously limited by the low  $FF$  (0.38).

As mentioned, a good EBL should effectively block excitons while allowing passage of electrons to the cathode. A good electron mobility is thus beneficial to the electron collection. Fig. 4 shows a plot of the  $J_{SC}$  against electron mobility of the EBL. Except for the case of  $m$ -PhPyCN, the  $J_{SC}$  shows an obvious increasing trend with the EBL's electron mobility, as expected. The low  $J_{SC}$  for the  $m$ -PhPyCN is likely to be related to its relatively shallow HOMO level and small energy gap, which weaken its exciton blocking ability.

It has been shown that the  $V_{OC}$  of an OPV device is mainly controlled by the energy offset at the donor/acceptor interfaces.<sup>39</sup> However, this is not considered to be a key variant in the present work, as all the devices have the same donor/acceptor interface and electrodes. It has also been shown that the  $V_{OC}$  is also a function of the dark current as described by eqn (1).<sup>40</sup>

$$V_{OC} = \frac{nkT}{q} \ln \left( \frac{J_{Ph} V_{OC}}{J_S} + 1 - \frac{V_{OC}}{R_{Sh} J_S} \right) \quad (1)$$

where  $J_S$  is the saturation dark current density (*i.e.* the saturation leakage current when the diode is reversely biased in dark),  $n$  is the ideality factor,  $R_{Sh}$  is the shunt resistance and  $J_{Ph}$  is the photocurrent. When  $J_{Ph}/J_S \gg 1$ ,  $V_{OC}$  is proportional to  $\ln(J_{Ph}/J_S)$ , suggesting that a large  $J_S$  would reduce the  $V_{OC}$ . This relation agrees well with our observation that the high  $V_{OC}$  of 0.53 and 0.51 V from the  $m$ -MPyCN and the  $p$ -PPTNT devices are accompanied by much smaller  $J_S$  of 0.00058 and

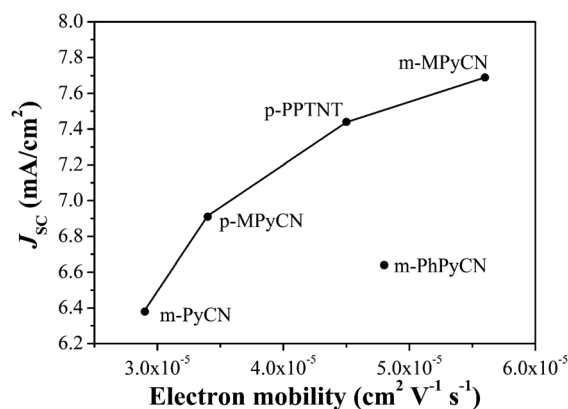


Fig. 4 The dependence of the  $J_{SC}$  on the electron mobility of the EBL.

Table 2 The device characteristics of the OPVs with different EBLs

EBL	$V_{OC}$ [V]	$J_{SC}$ [ $\text{mA cm}^{-2}$ ]	FF	PCE [%]	$R_S$ [ $\Omega \text{ cm}^2$ ]	$R_{Sh}$ [ $\Omega \text{ cm}^2$ ]	$J_S$ [ $\text{mA cm}^{-2}$ ]
BCP	0.47	6.33	0.50	1.47	52.29	289.16	0.0036
$m$ -PhPyCN	0.46	6.64	0.53	1.60	11.11	370.37	0.0035
$p$ -PPTNT	0.51	7.44	0.51	1.93	15.88	327.42	0.0013
$m$ -MPyCN	0.53	7.69	0.52	2.12	16.57	500.00	0.00058
$p$ -MPyCN	0.46	6.91	0.51	1.63	12.67	300.38	0.0030
$m$ -PyCN	0.46	6.38	0.52	1.55	11.93	472.44	0.0047
CNPyCN	0.45	6.21	0.38	1.07	25.61	156.25	0.0060

0.0013 mA cm<sup>-2</sup>, respectively, than the other devices. On the contrary, the CNPyCN device has the smallest  $V_{OC}$  of 0.45 V, corresponding to the highest  $J_S$  of 0.0060 mA cm<sup>-2</sup>. For other materials, similar  $V_{OC}$  are obtained as their  $J_S$  show relatively little variation.

We proceed to analyze the relationship between the  $J_S$  of the devices and the energy levels of the EBLs (Fig. 2 and Table 1). BCP has a HOMO energy of 6.5 eV, which is larger than that of C<sub>60</sub> (6.2 eV) just by 0.3 eV. On the other hand, *m*-MPyCN and *p*-PPTNT have HOMO energies of 6.91 and 6.81 eV, respectively, which are much larger than that of BCP and are beneficial for suppressing hole leakage. This in turn leads to lower  $J_S$  and thus higher  $V_{OC}$ . However, this simple picture cannot explain the cases for the *p*-MPyCN, *m*-PyCN and CNPyCN devices. Although their HOMO energy levels are deep enough to block holes effectively, their devices still have relatively high  $J_S$  and lower  $V_{OC}$ , indicating that there are other factors influencing the  $J_S$ .

One possible cause for the large  $J_S$  in the CNPyCN device is its low-lying LUMO energy level of 4.3 eV, which is much closer to the work function of Al (4.0 eV). This suggests that in reverse bias, electrons can possibly be injected from Al into the LUMO of CNPyCN. This is consistent with the observation that the leakage current of the CNPyCN device is considerably larger than those of the other devices. This also explains the smaller  $V_{OC}$  of the CNPyCN device. Early reports have demonstrated that the LUMO position of the EBL seems not to influence the photovoltaic performance due to the metal-deposition-induced damage for charge transport.<sup>41,42</sup> The present results suggest that there are possible situations where the  $J_S$  could be influenced when the offset between the EBL's LUMO and the cathode's work function is small. On the other hand, the causes of the relatively large  $J_S$  in the *p*-MPyCN and *m*-PyCN devices are not yet clear and require further investigations.

The FF is closely related to the series resistance ( $R_S$ ) and shunt resistance ( $R_{Sh}$ ) of OPVs. From Table 2, it can be seen that all devices using the new compounds show smaller  $R_S$  values than that of the reference device using BCP, indicating the higher electron mobilities of the cyano-substituted pyridine than that of BCP. With smaller  $R_S$  and larger  $R_{Sh}$  values than other devices, the FF of the devices using *m*-PhPyCN and *m*-PyCN reach 0.53 and 0.52, respectively. A FF of 0.52 was also achieved for the *m*-MPyCN device owing to its large  $R_{Sh}$  of 500 Ω cm<sup>2</sup>. For the CNPyCN device, it has a low FF of 0.38 and a relatively small  $R_{Sh}$  of 156.25 Ω cm<sup>2</sup>. The small  $R_{Sh}$  suggests that more carriers would be lost due to recombination and thus resulting in a small FF. Causes for the small  $R_{Sh}$  are not entirely clear yet. Nevertheless, this might be caused by more severe damage by Al cathode deposition on CNPyCN than on other materials. Further investigation is still needed to fully understand this.

### 3.5 Stability

As mentioned, the most important hurdle for commercialization of OPV devices is their poor stability. We have tested the device stability of the two compounds (*m*-MPyCN and *p*-PPTNT) with the highest electrical performance. Encapsulated devices using BCP, *m*-MPyCN and *p*-PPTNT as EBL were tested after different storage periods. As shown in Fig. 5, within 120 h the PCE of the BCP device has decreased to 0. On the other hand, the PCE of the

*p*-PPTNT device showed little decrease within 360 h and decreases by around 50% after 480 h. The *m*-MPyCN device shows a mild degradation within the first 240 h and still maintains about 50% of the initial PCE after 360 h. The poor stability of the BCP device can be attributed to its crystallization, leading to pin-holes and poor electrical conduction.<sup>16,20</sup> Therefore, thermal stability of the EBL is an important requirement to guarantee the device stability and lifetime, which has been proved by replacing BCP with materials of high  $T_g$ s. Thus, the stability of OPVs based on *p*-PPTNT and *m*-MPyCN were dramatically improved, maybe largely owing to their high  $T_g$ s of 139 and 149 °C, respectively. However, other factors that may affect the device stability are not yet clear and require further investigations.

## 4. Conclusions

In summary, a novel class of cyano-substituted pyridine derivatives has been designed and synthesized to meet the demand for EBLs. Most of them have high  $T_g$ s (139–189 °C), high electron mobilities (in the order of 10<sup>-5</sup> cm<sup>2</sup> V<sup>-1</sup> s<sup>-1</sup>) and deep HOMO energy levels (6.71–7.80 eV). With these properties, their applications as EBLs in small molecular lamellar OPVs were investigated. Devices with most of these cyano-substituted pyridine derivatives achieved better performance than that of BCP. In particular, a PCE up to 2.12% was obtained with *m*-MPyCN, which is about 44% higher than the BCP-based reference device. This performance enhancement is the best among all reported BCP replacements. The high electron mobility and suitable energy levels (including HOMO, LUMO and  $E_g$ ) of the present cyano-substituted pyridine derivatives account for the increases in  $J_{SC}$ ,  $V_{OC}$  and FF, and thus PCE in the corresponding devices. Considerably prolonged OPV lifetimes have also been demonstrated for *p*-PPTNT and *m*-MPyCN based devices, which may be mainly attributed to their high  $T_g$ s. The present results show that cyano-substituted pyridine would be potentially an important class of material for high-performance EBLs. The systematic studies here are also believed to provide useful guidance for the design of EBL materials.

## Acknowledgements

This work is financially supported by the National High Technology Research and Development Program of China

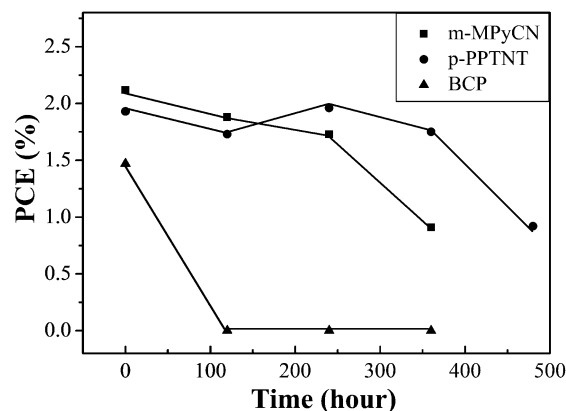


Fig. 5 PCE degradation of OPVs with *p*-PPTNT, *m*-MPyCN and BCP.

(863 Program) (Grant No. 2011AA03A110), the Beijing Natural Science Foundation (Grant No. 2111002), the National Natural Science Foundation of China (Grant No. 61178061), the Research Grants Council of Hong Kong (Grant No: CityU 101707).

## Notes and references

- 1 C. W. Tang, *Appl. Phys. Lett.*, 1986, **48**, 183.
- 2 G. Yu, J. Gao, J. C. Hummelen, F. Wudl and A. J. Heeger, *Science*, 1995, **270**, 1789.
- 3 P. Peumans, V. Bulovic and S. R. Forrest, *Appl. Phys. Lett.*, 2000, **76**, 2650.
- 4 H. Gommans, B. Verreet, B. P. Rand, R. Muller, J. Poortmans, P. Heremans and J. Genoe, *Adv. Funct. Mater.*, 2008, **18**, 3686.
- 5 V. Shrotriya, G. Li, Y. Yao, C. W. Chu and Y. Yang, *Appl. Phys. Lett.*, 2006, **88**, 073508.
- 6 Y. M. Hwang, S. J. Moon, W. W. So, S. C. Yoon, C. J. Lee and W. S. Shin, *Mol. Cryst. Liq. Cryst.*, 2008, **491**, 324.
- 7 M. F. Lo, T. W. Ng, S. L. Lai, M. K. Fung, S. T. Lee and C. S. Lee, *Appl. Phys. Lett.*, 2011, **99**, 033302.
- 8 G. Li, V. Shrotriya, J. S. Huang, Y. Yao, T. Moriarty, K. Emery and Y. Yang, *Nat. Mater.*, 2005, **4**, 864.
- 9 J. Peet, J. Y. Kim, N. E. Coates, W. L. Ma, D. Moses, A. J. Heeger and G. C. Bazan, *Nat. Mater.*, 2007, **6**, 497.
- 10 S. H. Park, A. Roy, S. Beaupre, S. Cho, N. Coates, J. S. Moon, D. Moses, M. Leclerc, K. Lee and A. J. Heeger, *Nat. Photonics*, 2009, **3**, 297.
- 11 N. Blouin, A. Michaud and M. Leclerc, *Adv. Mater.*, 2007, **19**, 2295.
- 12 Y. Y. Liang, Y. Wu, D. Q. Feng, S. T. Tsai, H. J. Son, G. Li and L. P. Yu, *J. Am. Chem. Soc.*, 2009, **131**, 56.
- 13 Y. Y. Liang, Z. Xu, J. B. Xia, S. T. Tsai, Y. Wu, G. Li, C. Ray and L. P. Yu, *Adv. Mater.*, 2010, **22**, E135.
- 14 T. W. Ng, M. F. Lo, Y. C. Zhou, Z. T. Liu, C. S. Lee, O. Kwon and S. T. Lee, *Appl. Phys. Lett.*, 2009, **94**, 193304.
- 15 K. S. Yook, S. O. Jeon, O. Y. Kim and J. Y. Lee, *Electrochem. Solid-State Lett.*, 2011, **14**, B59.
- 16 M. F. Lo, T. W. Ng, S. L. Lai, F. L. Wong, M. K. Fung, S. T. Lee and C. S. Lee, *Appl. Phys. Lett.*, 2010, **97**, 143304.
- 17 Q. L. Song, F. Y. Li, H. Yang, H. R. Wu, X. Z. Wang, W. Zhou, J. M. Zhao, X. M. Ding, C. H. Huang and X. Y. Hou, *Chem. Phys. Lett.*, 2005, **416**, 42.
- 18 Q. L. Song, M. L. Wang, E. G. Obbard, X. Y. Sun, X. M. Ding, X. Y. Hou and C. M. Li, *Appl. Phys. Lett.*, 2006, **89**, 251118.
- 19 Q. L. Song, C. M. Li, M. L. Wang, X. Y. Sun and X. Y. Hou, *Appl. Phys. Lett.*, 2007, **90**, 071109.
- 20 S. W. Liu, C. C. Lee, C. F. Lin, J. C. Huang, C. T. Chen and J. H. Lee, *J. Mater. Chem.*, 2010, **20**, 7800.
- 21 N. N. Wang, J. S. Yu, Y. Zang, J. Huang and Y. D. Jiang, *Sol. Energy Mater. Sol. Cells*, 2010, **94**, 263.
- 22 D. F. O'Brien, P. Burrows, S. R. Forrest, B. E. Koene, D. E. Loy and M. E. Thompson, *Adv. Mater.*, 1998, **10**, 1108.
- 23 S. J. Liu, F. He, H. Wang, H. Xu, C. Y. Wang, F. Li and Y. G. Ma, *J. Mater. Chem.*, 2008, **18**, 4802.
- 24 S. Bertho, G. Janssen, T. J. Cleij, B. Conings, W. Moons, A. Gadisa, J. D'Haen, E. Goovaerts, L. Lutsen, J. Manca and D. Vanderzande, *Sol. Energy Mater. Sol. Cells*, 2008, **92**, 753.
- 25 F. M. Hsu, C. H. Chien, Y. J. Hsieh, C. H. Wu, C. F. Shu, S. W. Liu and C. T. Chen, *J. Mater. Chem.*, 2009, **19**, 8002.
- 26 A. R. G. Smith, J. L. Ruggles, H. Cavaye, P. E. Shaw, T. A. Darwish, M. James, I. R. Gentle and P. L. Burn, *Adv. Funct. Mater.*, 2011, **21**, 2225.
- 27 N. Li, P. F. Wang, S. L. Lai, W. M. Liu, C. S. Lee, S. T. Lee and Z. T. Liu, *Adv. Mater.*, 2010, **22**, 527.
- 28 N. Li, S. L. Lai, W. M. Liu, P. F. Wang, J. J. You, C. S. Lee and Z. T. Liu, *J. Mater. Chem.*, 2011, **21**, 12977.
- 29 C. L. Li, S. J. Shieh, S. C. Lin and R. S. Liu, *Org. Lett.*, 2003, **5**, 1131.
- 30 G. Bringmann, A. J. P. Mortimer, P. A. Keller, M. J. Gresser, J. Garner and M. Breuning, *Angew. Chem., Int. Ed.*, 2005, **44**, 5384.
- 31 A. Mazzanti, L. Lunazzi, M. Minzoni and J. E. Anderson, *J. Org. Chem.*, 2006, **71**, 5474.
- 32 Y. R. Lai, L. Xing, G. I. Poda and Y. D. Hu, *Drug Metab. Dispos.*, 2007, **35**, 937.
- 33 S. H. Ye, Y. Q. Liu, C. A. Di, H. X. Xi, W. P. Wu, Y. G. Wen, K. Lu, C. Y. Du, Y. Liu and G. Yu, *Chem. Mater.*, 2009, **21**, 1333.
- 34 S. Barth, P. Muller, H. Riel, P. F. Seidler, W. Riess, H. Vestweber and H. Bassler, *J. Appl. Phys.*, 2001, **89**, 3711.
- 35 T. C. Wong, J. Kovac, C. S. Lee, L. S. Hung and S. T. Lee, *Chem. Phys. Lett.*, 2001, **334**, 61.
- 36 Z. Y. Xie, T. C. Wong, L. S. Hung and S. T. Lee, *Appl. Phys. Lett.*, 2002, **80**, 1477.
- 37 A. Moliton and J. M. Nunzi, *Polym. Int.*, 2006, **55**, 583.
- 38 Yuan Li, *Organic Photovoltaics Analysis Platform (OPVAP)*, www.OPVAP.inwake.com.
- 39 B. P. Rand, D. P. Burk and S. R. Forrest, *Phys. Rev. B: Condens. Matter Mater. Phys.*, 2007, **75**, 115327.
- 40 N. Li, B. E. Lassiter, R. R. Lunt, G. Wei and S. R. Forrest, *Appl. Phys. Lett.*, 2009, **94**, 023307.
- 41 Z. R. Hong, Z. H. Huang and X. T. Zeng, *Chem. Phys. Lett.*, 2006, **425**, 62.
- 42 B. P. Rand, J. Li, J. G. Xue, R. J. Holmes, M. E. Thompson and S. R. Forrest, *Adv. Mater.*, 2005, **17**, 2714.